

Outer-gap vs. Slot-gap Models for Pulsar High Energy Emissions: The Case of the Crab Pulsar

Kouichi Hirotani

ASIAA/National Tsing Hua University - TIARA,
PO Box 23-141, Taipei, Taiwan¹

hirotani@tiara.sinica.edu.tw

ABSTRACT

We analytically examine the capabilities of rotation-powered pulsars as the sources of gamma-rays and show that their phase-averaged gamma-ray flux is proportional to the product of the spin-down flux and the gap trans-field thickness cubed irrespective of the emission models. Applying the scheme to the Crab pulsar, we demonstrate that the outer-gap model reproduces the observed GeV fluxes and that the slot-gap model reproduces at most twenty per cent of the observed fluxes because of the small trans-field thickness. An implication on the relationship between the gamma-ray and the spin-down fluxes is discussed.

Subject headings: gamma-rays: observations – gamma-rays: theory – magnetic fields – methods: analytical – pulsars: individual(Crab)

1. Introduction

The launch of Fermi Gamma-ray Space Telescope will soon open a new era for the studies of rotation-powered pulsars. The unprecedented sensitivity and spectral resolution of the Large Area Telescope (LAT) aboard Fermi Space Telescope will allow for detailed studies of particle acceleration and radiation in rotating neutron-star (NS) magnetospheres. To make the best use of the power of LAT observations, we need the most sophisticated model with minimum assumptions.

In all the pulsar emission models, e^- 's and/or e^+ 's are accelerated by the magnetic-field-aligned electric field, E_{\parallel} , to radiate photons in the open zone (fig. 1 in Hirotani 2008, hereafter H08) mainly via synchro-curvature process. In polar-cap (PC) models, emission takes place within several NS radii above a PC surface (Arons & Scharlemann 1979; Daugherty & Harding 1982, 1996). However, such a low-altitude emission predicts too small beam size to produce the observed

wide pulse profiles. Therefore, extending the original idea by Arons (1983), Muslimov and Harding (2003, hereafter MH03; 2004a, b) and Dyks et al. (2004, hereafter DHR04) sought the possibility of a wide hollow cone of high-energy radiation due to the flaring of field lines. They proposed the slot-gap (SG) model, in which emission takes place along the last-open field lines. Recently, Harding et al. (2008, hereafter HSDF08) demonstrated that the SG model reasonably reproduces the Crab pulsar phase-resolved spectrum (Fierro et al. 1998; Kuiper et al. 2001; Nolan et al. 1993).

The outer-gap (OG) model gives an alternative possibility (Cheng et al. 1986a,b; Romani 1996; Cheng & Zhang 1996; Hirotani 2006a, b, hereafter H06a, b). It differs from the SG model in the following ways: • An OG extends between the null surface on which the magnetic field becomes perpendicular to the rotation axis and the light cylinder on which the plasma co-rotational velocity would exceed the speed of light, c . A SG extends between the PC surface and the light cylinder. • For Crab, an OG occupies more than 10% of the open magnetic fluxes with a large electrostatic potential drop, $\Delta\Psi \sim 10^{15}$ V, whereas a

¹Postal address: TIARA, Department of Physics, National Tsing Hua University, 101, Sec. 2, Kuang Fu Rd., Hsinchu, Taiwan 300

SG occupies several % of the open fluxes with $\Delta\Psi \sim 10^{13}$ V. • Pair production copiously takes place in OGs, whereas it is negligible in SGs.

The purpose here is to explore further into the two models. We examine their common emission properties in § 2, and separately consider the OG and SG models in §§ 3 and 4. § 5 is for discussion.

2. Gamma-ray Flux

In this letter, we concentrate on the *phase-averaged* spectrum of pulsar magnetospheric emissions, sacrificing the examinations of light curves and phase-resolved spectra. In this context, we can neglect the aberration of photon propagation directions and the time-of-flight delay due to different emission altitudes from the NS, because these two relativistic effects do not change the total number of photons to be detected. Although this thought experiment does not describe any realistic pulsar emissions, it significantly reduces the calculation of photon propagations and gives the correct *phase-averaged* spectrum.

To investigate the upper limit of photon fluxes, we neglect photon absorptions. Then the radiative transfer equation gives the specific intensity $I_\nu \approx 2b\varrho_c j_\nu$, where $b \approx \gamma^{-1}$ denotes the emission beaming angle, γ the Lorentz factor of e^\pm 's, ϱ_c the local curvature radius of the magnetic field line, j_ν the emission coefficient, and $2b\varrho_c$ the distance interval from which the photons are detected by the observer (fig. 6.2 in Rybicki & Lightman 1979). Giving the emission coefficient as $j_\nu \approx N(dP/d\nu)/(\pi b^2)$, we obtain

$$I_\nu \approx \frac{2}{\pi} \frac{\varrho_c}{b} N \frac{dP}{d\nu}, \quad (1)$$

where N denotes the spatial density of e^- 's or e^+ 's, and $dP/d\nu$ the radiation power per particle.

At each magnetic azimuth φ_* on the PC surface, we parameterize the field-line footpoint with their magnetic colatitude θ_* measured from the magnetic axis. We define that the primary photons are emitted only along the field lines threading the PC surface with $\theta_*^{\min} < \theta_* < \theta_*^{\max}$, where the upper boundary and the last-open field lines are designated with θ_*^{\min} and θ_*^{\max} , respectively. We further introduce the dimensionless gap trans-field thickness, $h_m \equiv (\theta_*^{\max} - \theta_*^{\min})/\theta_*^{\max}$. In this letter, we assume that h_m is constant for both φ_*

and s (distance along the field line) for simplicity.

Let us introduce the gap meridional thickness Δz that represents the distance between the last-open field line and the upper boundary measured perpendicularly to the field line. Then, the observer detects emissions from the magnetic-flux cross section $\Delta A \approx \Delta z \times 2br \sin \theta$, where $r \sin \theta$ refers to the distance from the magnetic axis, and $2b$ the *azimuthal* full opening angle of the points from which the photons propagate towards the observer. For an aligned rotator, the azimuthal length from which the photons propagate towards the observer is given by $2br \sin \theta$; thus, $\Delta A = \Delta z \times 2br \sin \theta$ holds. For an oblique rotator, in the outer magnetosphere, toroidal expansion of the field line flux tubes is similar to an aligned case; thus, $\Delta A \approx \Delta z \times 2br \sin \theta$ approximately holds. Since $\Delta z \approx 2h_m \varpi_{\text{LC}} (r/\varpi_{\text{LC}})^2 \csc \theta (1 + 3 \cos^2 \theta)^{-1/2}$ holds for a dipole field, we obtain

$$\Delta A \approx 2bh_m \varpi_{\text{LC}}^2 (B_*/B) (r_*/\varpi_{\text{LC}})^3, \quad (2)$$

where r denotes the distance from the NS center, θ the magnetic colatitude, $\varpi_{\text{LC}} \equiv c/\Omega$ the light cylinder radius, Ω the NS angular frequency. The magnetic field strength B is evaluated at the emission point and related with its surface value B_* by $B/B_* = (r_*/r)^3 \sqrt{1 + 3 \cos^2 \theta}/2$.

The photon energy flux can be computed by

$$\nu F_\nu = \nu I_\nu (\Delta A/d^2), \quad (3)$$

where d is the distance to the pulsar. Substituting equations (1) and (2) into equation (3), we obtain

$$\nu F_\nu \approx \frac{4}{\pi} h_m \frac{\Omega B_*}{2\pi c e} n \varrho_c \nu \frac{dP}{d\nu} \left(\frac{r_*}{d}\right)^2 \frac{r_*}{\varpi_{\text{LC}}}, \quad (4)$$

where e is the charge on the positron; the dimensionless particle density per magnetic flux tube, $n \equiv (2\pi c e/\Omega B)N$, becomes approximately $\cos \alpha_i$, where α_i is the magnetic inclination with respect to the rotation axis. The quantity $\Omega B_*/(2\pi c e)$ expresses the typical Goldreich-Julian (GJ) particle number density at the PC surface (Goldreich & Julian 1969). It follows from equation (4) that the photon flux νF_ν does not depend on b .

For saturated e^- 's or e^+ 's, electrostatic force balance, $eE_\parallel = 2e^2\gamma^4/(3\varrho_c^2)$, gives the terminal Lorentz factor

$$\gamma = 2.20 \times 10^5 \Omega_2^{-1/2} \left(\frac{\varrho_c}{0.5\varpi_{\text{LC}}}\right)^{1/2} \left(\frac{E_\parallel}{\text{V m}^{-1}}\right)^{1/4}, \quad (5)$$

where $\Omega_2 \equiv \Omega/(10^2 \text{ rad s}^{-1})$ and $E_{\parallel} \equiv -(\mathbf{B}/B) \cdot \nabla \Psi$. The non-corotational potential Ψ is given by the inhomogeneous part of the Maxwell equations,

$$-\nabla^2 \Psi = 4\pi(\rho - \rho_{\text{GJ}}) = (2\Omega B_z/c)\kappa, \quad (6)$$

where ρ and ρ_{GJ} denote the real and GJ charge densities, respectively, and B_z the magnetic field component projected along the rotation axis. The effective charge density, $\rho_{\text{GJ}} - \rho$, is parameterized by κ , which is a function of position. In the Newtonian limit, we would have $\kappa = 1$ for a vacuum gap while $\kappa < 1$ for a non-vacuum gap.

Since e^{\pm} 's are ultra-relativistic in the gap, the primary emission is dominated by the pure-curvature component. Thus,

$$\nu \frac{dP}{d\nu} = \frac{3\sqrt{3}}{4\pi} \frac{ce^2\gamma^4}{\varrho_c^2} x^2 \int_x^{\infty} K_{5/3}(\xi) d\xi \quad (7)$$

peaks at $x \equiv \nu/\nu_c = 1.318$ with the maximum value $x^2 \int_x^{\infty} K_{5/3}(\xi) d\xi = 0.6826$, where $K_{5/3}$ is the modified Bessel function of 5/3 order, and $\nu_c \equiv (3/4\pi)(c\gamma^3/\varrho_c)$ the characteristic frequency of the emission. The electrostatic force balance, $(2/3)e^2\gamma^4/\varrho_c^2 = eE_{\parallel}$, gives

$$\nu \frac{dP}{d\nu} = \frac{9\sqrt{3}}{8\pi} ceE_{\parallel} x^2 \int_x^{\infty} K_{5/3}(\xi) d\xi. \quad (8)$$

For a thin gap ($h_m \ll 1$), equation (68) in H06a gives

$$E_{\parallel} \approx \frac{h_m^2}{4} \left(\frac{r_*}{\varpi_{\text{LC}}} \right)^3 B_* \frac{\partial(-\kappa B_z/B)}{\partial(s/\varpi_{\text{LC}})}, \quad (9)$$

where s is the distance along the field line. For the field lines curving away (or toward) the rotation axis, $1.0 < -\partial(B_z/B)/\partial(s/\varpi_{\text{LC}}) < 1.5$ (or $1.5 < -\partial(B_z/B)/\partial(s/\varpi_{\text{LC}}) < 2.2$) is the typical range.

Substituting $B_* = 2\mu/r_*^3$ and $x^2 \int_x^{\infty} K_{5/3}(\xi) d\xi = 0.68$, and combining equations (4), (8) and (9), we finally obtain the peak flux,

$$(\nu F_{\nu})_{\text{peak}} \approx 0.0450 f h_m^3 \kappa \frac{\mu^2 \Omega^4}{c^3} \frac{1}{d^2} \quad (10)$$

where μ denotes the magnetic dipole moment and

$$f \equiv \frac{n}{0.7} \frac{\varrho_c}{0.5\varpi_{\text{LC}}} \frac{1}{1.5\kappa} \frac{\partial(-\kappa B_z/B)}{\partial(s/\varpi_{\text{LC}})} \quad (11)$$

is close to unity (see also Zhang & Cheng 2003). If we apply $\int_0^{\infty} x \int_x^{\infty} K_{5/3}(\xi) d\xi = 1.61$, we

also obtain the integrated flux, $\int_0^{\infty} F_{\nu} d\nu = 2.36(\nu F_{\nu})_{\text{peak}}$. Note that the factor $\mu^2 \Omega^4/(c^3 d^2)$ is proportional to the spin-down flux (§ 5).

It should be emphasized that equation (10) estimates the upper limit of the phase-averaged flux. For example, for an axisymmetric gap in an aligned rotator ($\alpha_i = 0^\circ$), the phase-averaged flux equals equation (10), which is constant during the whole NS rotation. Since equation (10) holds particularly well for an aligned rotator, and since the phase-averaged flux decreases with increasing α_i (e.g., MH03 and DHR04), equation (10) gives the upper limit for general α_i . The actual flux will be a few times less than equation (10), because only the field lines in a limited azimuthal range are active, and because the ρ_{GJ} at the PC surface decreases with increasing α_i . In § 4, we confirm this by comparing with numerical results.

The difference between the OG and the SG models comes into equation (10) through h_m , κ , and the assumed μ . In §§ 3 and 4, we apply this equation to these two models, considering the brightest spin-down-flux pulsar, the Crab pulsar, assuming $d = 2$ kpc.

3. Outer-gap Model

First, let us apply equation (10) to the OG models. Using the vacuum ($\kappa = 1.0$) OG models of Cheng et al. (2000), Takata et al. (2008) and Tang et al. (2008), which proposed $h_m \approx 0.11$ (i.e., $f \approx 0.11$ in their notation), we obtain

$$(\nu F_{\nu})_{\text{peak}} \approx 6.58 \times 10^{-4} f \kappa \left(\frac{h_m}{0.11} \right)^3 \left(\frac{\mu_{30}}{3.8} \right)^2 \text{ MeV s}^{-1} \text{ cm}^{-2}, \quad (12)$$

with $E_{\parallel} \approx 2.55 \times 10^8 \text{ V m}^{-1}$, $\gamma \approx 2.0 \times 10^7$, where $\mu_{30} \equiv \mu/(10^{30} \text{ G cm}^3)$. The νF_{ν} flux peaks at $1.3h\nu_c \approx 4.1 \text{ GeV}$. These results are consistent with their vacuum OG models and with the observed phase-averaged spectrum, where the photon flux around GeV is dominated by the primary curvature component rather than the reprocessed synchrotron-self-Compton one (Takata & Chang 2007). Exactly speaking, the vacuum OG model is not self-consistent electro-dynamically, because it assumes a vanishing charge density while it adopts the GJ flux of radiating e^{\pm} 's. If one instead adopts the actual e^+ flux in a (nearly)

vacuum OG, the predicted γ -ray flux would be a few orders of magnitude less than equation (12) (left panel of fig. 8 in H06a). That is, equation (12), and hence the traditional OG models reproduce observations only phenomenologically.

Secondly, let us consider the non-vacuum OG solution, which consistently takes the pair production in the pulsar magnetosphere into account. Using $\kappa \approx 0.3$ and $h_m \approx 0.14$, we obtain

$$(\nu F_\nu)_{\text{peak}} \approx 4.06 \times 10^{-4} f \frac{\kappa}{0.3} \left(\frac{h_m}{0.14} \right)^3 \left(\frac{\mu_{30}}{3.8} \right)^2 \text{ MeV s}^{-1} \text{ cm}^{-2}, \quad (13)$$

which is consistent with the numerical results for Crab (figs. 8 & 9 in H08). In short, the OG model reproduces the observed flux around GeV.

4. Slot-gap Model

Thirdly, let us apply equation (10) to the SG model, which adopts $h_m < 0.05$ (i.e., $\Delta\xi_{\text{SG}} < 0.05$ in HSDF08's notation) and $\kappa \approx -(0.1 + 0.2s/\varpi_{\text{LC}})$ for the Crab pulsar. At the outer part ($s \approx 0.6\varpi_{\text{LC}}$), where emissivity is large, we obtain

$$(\nu F_\nu)_{\text{peak}} \approx 6.02 \times 10^{-5} f \frac{\kappa}{0.22} \left(\frac{h_m}{0.05} \right)^3 \left(\frac{\mu_{30}}{8} \right)^2 \text{ MeV s}^{-1} \text{ cm}^{-2}, \quad (14)$$

with $|E_\parallel| \approx 2.4 \times 10^7 \text{ V m}^{-1}$ and $\gamma \approx 1.1 \times 10^7$.

If we adopt the same parameter set $h_m = 0.04$ and $\mu_{30} = 11$ as HSDF08, and if we adopt $|E_\parallel| \approx 7 \times 10^6 \text{ V m}^{-1}$, which is derived from the potential drop $0.5 \times 1.3 \times 10^{13} \text{ V}$ in the higher altitudes SG (HSDF08), equations (4) and (8) give $(\nu F_\nu)_{\text{peak}} \approx 1.9 \times 10^{-5} \text{ MeV s}^{-1} \text{ cm}^{-2}$. This analytical prediction can be confirmed by a numerical computation of the 3-D SG model (H08). If we adopt the same parameter set as HSDF08 and if we adopt the same E_\parallel as their equation (4) for $\alpha_i = 45^\circ$, we obtain the photon map as figure 1, which shows a caustic emission from the higher altitudes by virtue of the exclusion of the strong lower-altitude emission. Specifying the observer's viewing angle with respect to the rotation axis, and integrating over the entire NS rotation, we obtain the phase-averaged spectrum (fig. 2), which lies much below the observed value. Since $|E_\parallel| \approx 7 \times 10^6 \text{ V m}^{-1}$ gives $\gamma \approx 8.3 \times 10^6$

(eq. [5]), we interpret that HSDF08, who adopted $\gamma \sim 2 \times 10^7$, overestimated $(\nu F_\nu)_{\text{peak}}$ by the factor $(2/0.83)^4 \sim 33$.

Equation (14) could give the observed flux if $\mu_{30} > 17$. However, such a large μ_{30} is not allowed in recent analyzes of force-free electrodynamics. For example, Spitkovsky (2006) derived $\dot{E} \equiv I\Omega\dot{\Omega} \approx (\mu^2\Omega^4/c^3)(1 + \sin^2\alpha_i)$, where I denotes the NS moment of inertia and $\dot{\Omega}$ the temporal derivative of Ω . Imposing $I_{45} \equiv I/(10^{45} \text{ g cm}^3) < 5$ (with $r_* = 16 \text{ km}$ and $M < 2.5M_\odot$; e.g., Lattimer & Prakash 2000), we obtain $\mu_{30} < 3.10\sqrt{I_{45}} < 7.07$ for Crab. Thus, even HSDF08's value, $\mu_{30} = 11$, may be a little too large. In short, equation (14) gives the conservative upper limit and the SG model can explain at most 20% of the observed flux.

5. Discussion

If we assume that the spin down follows the dipole radiation formula, $\dot{E} = 2\mu^2\Omega^4 \sin^2\alpha_i/(3c^3)$, equation (10) becomes

$$(\nu F_\nu)_{\text{peak}} \approx 0.0954 f h_m^3 \kappa \frac{\dot{E}}{d^2} \frac{0.707}{\sin^2\alpha_i}, \quad (15)$$

where \dot{E}/d^2 denotes the spin-down flux at the Sun. It was, therefore, natural that the largest spin-down-flux pulsars were preferentially detected with the Energetic Gamma Ray Experiment Telescope (EGRET). The same tendency can be predicted for Fermi Space Telescope.

For young pulsars, both h_m and κ are less than unity (e.g., $h_m \approx 0.1$ and $\kappa \approx 0.3$ for Crab) owing to the copious pair production in the magnetosphere. As a result, $\int_0^\infty F_\nu d\nu$ becomes much less than \dot{E}/d^2 as demonstrated by H08. For middle-aged pulsars, on the contrary, $h_m > 0.5$ and $\kappa \approx 1$ holds (Hirotani et al. 2003), leading to an increasing ratio of $\int_0^\infty F_\nu d\nu/(\dot{E}/d^2)$ with age.

To explain the observed relationship $\int_0^\infty F_\nu d\nu \propto (\dot{E}/d^2)^{0.5}$ of pulsed γ -ray emissions (Thompson et al. 1994; Nel et al. 1996), it is essential to examine the evolution of h_m with age. From equation (10), we can at least state that the index α defined by $\int_0^\infty F_\nu d\nu \propto (\dot{E}/d^2)^\alpha$ becomes less than unity, because h_m increases with decreasing \dot{E} , as discussed just above. To examine the evolution of h_m , we must solve the screening of E_\parallel due to the discharge of the produced pairs in 3-D pulsar mag-

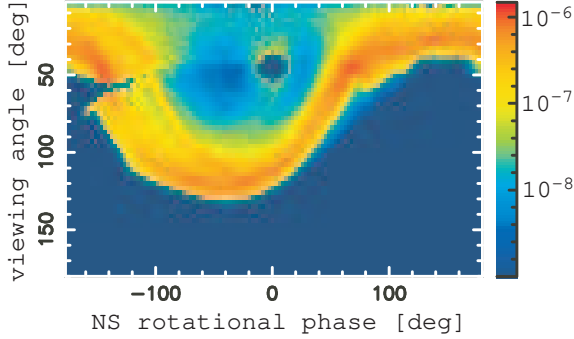


Fig. 1.— 3-D SG prediction: Photon flux per phase [$\text{MeV s}^{-1} \text{cm}^{-2} \text{deg}^{-1}$] at distance $d = 2$ kpc from the Crab pulsar as a function of the viewing angle and the phase. Only the emission from the SG connected to the north pole (i.e., one of the two SGs) is depicted for clarity.

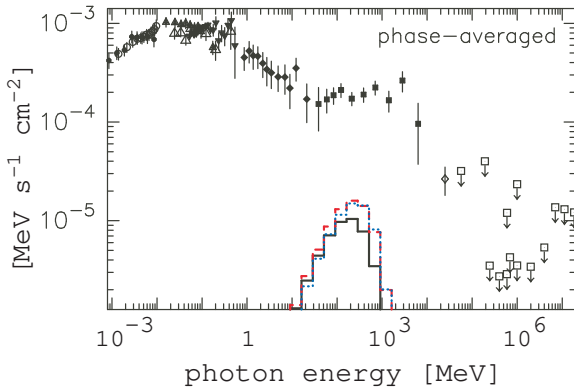


Fig. 2.— 3-D SG prediction: Crab phase averaged spectrum at three discrete viewing angles: 100° (solid), 110° (dashed), and 120° (dotted). Emission from both SGs are considered. For observational data points, see Kuiper et al. (2001, and references therein), and Aliu et al. (2008) for the flux at 25 GeV.

netospheres. In subsequent papers, we shall look more carefully into this issue, by simultaneously solving equation (6), the Boltzmann equations for e^\pm 's, and the radiative transfer equation under minimum assumptions.

The author is grateful to Drs. A. K. Harding, B. Rudak (the reviewer), K. S. Cheng, H. K. Chang, and J. Takata for helpful suggestions. This work is supported by the Theoretical Institute for Advanced Research in Astrophysics (TIARA) operated under Academia Sinica and the National Science Council Excellence Projects program in Taiwan administered through grant number NSC 96-2752-M-007-006-PAE.

REFERENCES

- Aliu, E. et al. 2008, Science in press (astro-ph/0809.2998)
- Arons, J. 1983, ApJ 302, 301
- Arons, J., Scharlemann, E. T. 1979, ApJ 231, 854
- Cheng, K. S., Ho, C., & Ruderman, M., 1986a ApJ, 300, 500 (CHR86a)
- Cheng, K. S., Ho, C., & Ruderman, M., 1986b ApJ, 300, 522 (CHR86b)
- Cheng, K. S., & Zhang, L. 1996, ApJ463, 271
- Cheng, K. S., Ruderman, M., & Zhang, L. 2000, ApJ, 537, 964
- Daugherty, J. K., & Harding, A. K. 1982, ApJ, 252, 337
- Daugherty, J. K., & Harding, A. K. 1996, ApJ, 458, 278
- Dyks, J., Harding, A. K., & Rudak, B. 2004, ApJ606, 1125 (DHR04)
- Fierro, J. M. et al. 1998, ApJ494, 734
- Goldreich, P. Julian, W. H. 1969, ApJ. 157, 869
- Harding, A. K. et al. 2008, ApJ, 680, 1378 (HSDF08)
- Hirota, K. 2006, ApJ652, 1475 (H06a)
- Hirota, K. 2006, Mod. Phys. Lett. A (Brief Review) 21, 1319–1337 (H06b)

- Hirovani, K. 2008, submitted to the Open Astron. J. astro-ph/0809.1283 (H08)
- Hirovani, K., Harding, A. K., & Shibata, S., 2003, ApJ591, 334 (HHS03)
- Kuiper, L. et al. 2001, A& A 378, 918
- Lattimer, J. M., & Prakash, M. 2000, Phys. Rep. 333, 121
- Muslimov, A. G., & Harding, A. K., 2003, ApJ, 588, 430 (MH03)
- Muslimov, A. G., & Harding, A. K., 2004a, ApJ, 606, 1143 (MH04a)
- Muslimov, A. G., & Harding, A. K., 2004b, ApJ, 617, 471 (MH04b)
- Nel, H. I., et al. ApJ465, 898.
- Nolan, P. L., et al. 1993, ApJ409, 697
- Romani, R. W. 1996, ApJ, 470, 469
- Rybicki, G. B., & Lightman, A. P. 1979, Radiative Processes in Astrophysics (New York: John Wiley & Sons)
- Spitkovsky, A. 2006, ApJ 648, L51
- Takata, J., & Chang, H.-K., 2007, ApJ670, 677
- Takata, J., Chang, H. K., & Shibata, S., 2008, MNRAS386, 748
- Tang, A. P. S. et al. 2008, ApJ676, 562.
- Thompson, D. J., et al. 1994, ApJ436, 229
- Zhang, L. Cheng, K. S. 2003, A&A 398, 639